ACS APPLIED MATERIALS & INTERFACES

Research Article

www.acsami.org

Detection of Vulnerable Atherosclerosis Plaques with a Dual-Modal Single-Photon-Emission Computed Tomography/Magnetic Resonance Imaging Probe Targeting Apoptotic Macrophages

Dengfeng Cheng,[†,‡] Xiao Li,[†,‡] Chunfu Zhang,[§] Hui Tan,[†,‡] Cong Wang,[∥] Lifang Pang,[†,‡] and Hongcheng Shi*[,†,‡]

[†]Department of Nuclear Medicine and [∥]Shanghai Institute of Cardiovascular Diseases, Zhongshan Hospital, Fudan University, Shanghai 200032, China

[‡]Shanghai Institute of Medical Imaging, Shanghai 200032, China

[§]School of Biomedical Engineering & Med-X Research Institute, Shanghai Jiao Tong University, Shanghai 200030, China

ABSTRACT: Atherosclerosis (AS), especially the vulnerable AS plaque rupture-induced acute obstructive vascular disease, is a leading cause of death. Accordingly, there is a need for an effective method to draw accurate predictions about AS progression and plaque vulnerability. Herein we report on an approach to constructing a hybrid nanoparticle system using a single-photon-emission computed tomography (SPECT)/magnetic resonance imaging (MRI) multimodal probe, aiming for a comprehensive evaluation of AS progression by achieving high sensitivity along with high resolution. Ultrasmall superparamagnetic iron oxide (USPIO) was covered by aminated poly(ethylene glycol) (PEG) and carboxylated PEG simultaneously and then functionalized with diethylenetriaminepentacetate acid for ^{99m}Tc coordination and subsequently Annexin V for targeting apoptotic macrophages abundant in vulnerable plaques. The in vivo accumulations of imaging probe reflected by SPECT and MRI were consistent and accurate in highlighting lesions. Intense radioactive signals detected by SPECT facilitated focus recognization and quantification, while USPIO-based T2-weighted MRI improved the focal localization and volumetry of AS plaques. For subsequent ex vivo planar images, targeting effects were further confirmed by immunohistochemistry, including CD-68 and TUNEL staining; meanwhile, the degree of concentration was proven to be statistically correlated with the Oil Red O staining results. In conclusion, these results indicated that the Annexin V-modified hybrid nanoparticle system specifically targeted the vulnerable AS plaques containing apoptotic macrophages and could be of great value in the invasively accurate detection of vulnerable plaques.

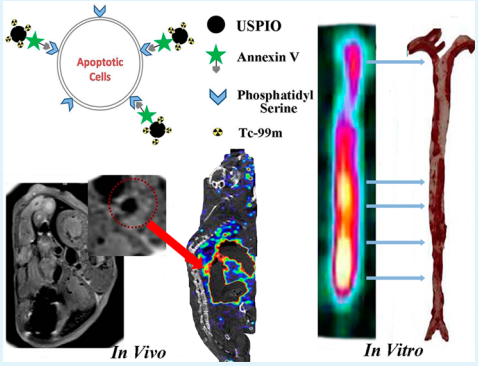

KEYWORDS: *SPECT/MRI, hybrid nanoparticle system, Annexin V, atherosclerosis, vulnerable plaque, apoptotic macrophage*

INTRODUCTION

Atherosclerosis (AS) is a common cardiovascular disease that develops and progresses slowly throughout life. Vulnerable AS plaque rupture-induced myocardial infarction, sudden cardiac death, and other acute obstructive vascular diseases seriously harm human health. It is difficult to draw accurate predictions about AS progression, especially the plaque vulnerability, from conventional angiography and ultrasonography. Although nuclear medical imaging such as ^{18}F-FDG and ^{11}C-Cholin can image inflammatory AS plaques, the relatively low specificity limits their clinical practice as well.[1] Recently, multimodal imaging, which combines two or more modalities of magnetic resonance imaging (MRI), fluorescence imaging, nuclear medical imaging, computed tomography (CT), and quantum-dots-based fluorescence, was proposed and demonstrated as an effective imaging pattern to improve specificity and resolution.[2−4] Therefore, a more specific targeting probe and conjugated imaging modalities for vulnerable plaque imaging are needed for a comprehensive evaluation of AS progression.

To design a more specific probe, selection of the appropriate target is a principal component to be considered. Because inflammation and apoptosis in the initial stage and progressive development are the main references, some relevant targeting molecules have been proposed and further verified via nuclear medical techniques. During the initial stage, ^{124}I/^{99m}Tc/^{123}I/^{111}In-labeled low-density lipoproteins (LDLs) specifically target the LDL receptor in AS plaques.[5,6] Similarly, throughout the entire AS process, ^{125}I/^{99m}Tc-MCP-1, ^{111}In monocytes, and ^{99m}Tc-B2702 (VCAM-1) specifically target the inflammation-associated factors, utilizing a highly expressed receptor or specific immunity.[7] Recently, ^{99m}Tc-Annexin V, ^{111}In/^{125}I angiogenesis, ^{99m}Tc-ASONs were developed for targeting apoptosis, the progressive change of macrophages that abundantly exist in vulnerable plaques.[8−10] Among these

Received: November 19, 2014
Accepted: January 8, 2015
Published: January 8, 2015

DOI: 10.1021/am508118x
ACS Appl. Mater. Interfaces 2015, 7, 2847−2855

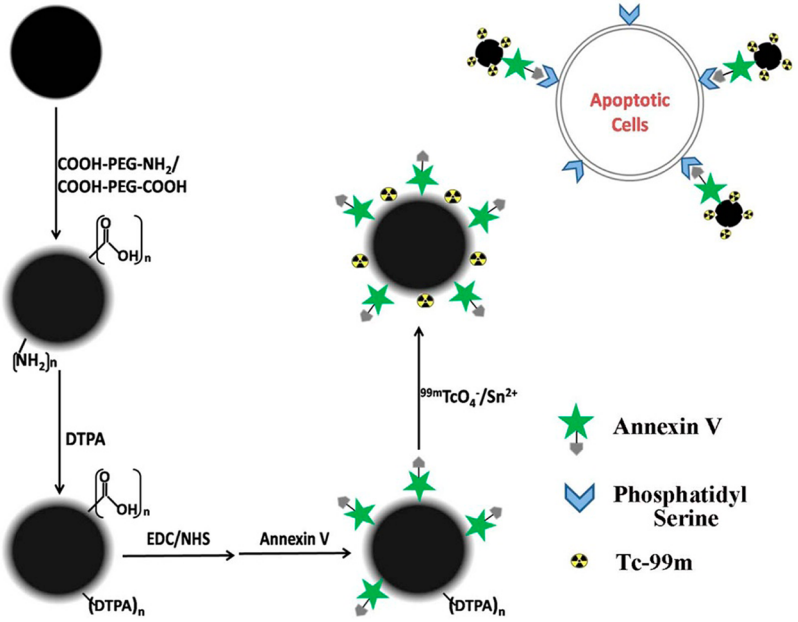

Figure 1. Schematic presentation of the procedures for preparing ^{99m}Tc−DTPA−USPIO−Annexin V. USPIO underwent PEG covering, DTPA conjugation, Annexin V conjugation, and ^{99m}Tc labeling. The targeting mechanism of a combination of probes and apoptotic cells is shown as well.

molecular imaging probes, ^{99m}Tc-Annexin V closely correlates with the amount of macrophages and the degree of apoptosis because of the pathologically confirmed intense macrophage inflammatory response and the strong correlation between the vulnerability and quantity of macrophage. As a targeting molecule, Annexin V efficiently recognizes phosphatidylserine (PS) located on the cytoplasmic surface of apoptotic cell membrances. Meanwhile, Annexin V has been shown to have an appropriate clearing speed in the blood system.[11] Additionally, the ^{99m}Tc-Annexin V uptake ratio of the advanced stage to the initial stage has been demonstrated to be 5−6 times higher than that of ^{18}F-FDG.[12] Besides AS, ^{99m}Tc-Annexin V was used to image apoptosis in vivo for such conditions as tumor treatment and neonatal hypoxic brain injury.[13]

Although the radiolabeled Annexin V-based nuclear imaging is of high specificity, there are obvious shortcomings as well. Because of its low resolution, nuclear medical imaging is not sensitive to small focus, easily leading to false negative diagnosis. However, radiolabeled hybrid superparamagnetic nanoparticle system-based multimodal imaging may solve this problem by integrating the properties of nuclear medical imaging with those of MRI to acquire both the high specificity of functional imaging and high resolution of structural imaging.

Because of biocompatibility and nontoxicity, ultrasmall superparamagnetic iron oxide (USPIO, composition of Fe_3O_4) is a versatile platform for constructing MRI-relevant multimodal imaging probes.[14−16] Annexin V-modified USPIO has been widely reported as efficient in apoptosis-related diseases as a MRI contrast agent.[17−19] In an in vitro phantom, Annexin V-IO can recognize >99% apoptotic cells in a mixture of Jurkat T cells; a significant T2-signal decrease of apoptotic cells relative to the control was observed even at 0.1 μg/mL.[20] Targeting capacities of Annexin V in nuclear medical imaging and MRI state the potential of Annexin V in multimodal imaging as the targeting molecule. Furthermore, the USPIO-based hybrid nanoparticle system has been extensively used in multimodal imaging, such as ^{99m}Tc-bisphosphonate-IO as a single-photon-emission computed tomography (SPECT)/MRI probe,[21] SPIO-PEG-folic acid in tumor imaging,[22] and RGD-PASP-IO as a positron emission tomography (PET)/MRI probe in tumor imaging.[23] Therefore, an Annexin V-functionalized USPIO-based hybrid nanoparticle system is a sound choice for vulnerable AS plaque-specific multimodal imaging.

In the present study, a facile synthesis route of an Annexin V-based hybrid nanoparticle system was designed so as to combine nuclear medical imaging and MRI. Annexin V attached to USPIO affords a strategy for the development of a SPECT/MRI probe for detecting apoptosis. Meanwhile, radionuclear ^{99m}Tc in this system is used for single photon emission. In order to simplify the procedures and stabilize the system, the noncytotoxic poly(ethylene glycol)s (PEGs) were used to fully cover the nanoparticles, while diethylenetriaminepentacetate acid (DTPA) was introduced to the USPIO surface for radionuclear labeling. To the best of our knowledge, there is no report on the research of dual-modal SPECT/MRI application in the diagnosis of vulnerable AS plaques. To validate this SPECT/MRI probe, high-fat diet-induced Apolipoproteins E knock out (ApoE$^{-/-}$) mice were selected as AS model animals and normal C57 mice were recruited as controls.

MATERIALS AND METHODS

Materials and Reagents. The following instruments were used: NanoSPECT/CT (Bioscan, Washington, DC); breast-specific γ imaging camera (BSGI; Dilon 6800 γ camera, Dilon Technologies, Newport News, VA); radioactivity meter (CRC-15R, Capintec Inc., Ramsey, NJ); micro-PET/CT (Inveon, Siemens Medical Solutions, Knoxville, TN); radio-thin-layer chromatography (RTLC; AR2000, Bioscan, Washington, DC); centrifuge (TGL-1613, Shanghai Anting Scientific Instrument Factory, Shanghai, China); transmission electron microscope (TEM; 2100F, JEOL Ltd. Tokyo, Japan); zetasizer Nano (ZSP, Malvern Instruments Ltd., Worcestershire, U.K.).

The following materials and reagents were used: 1-ethyl-3-[3-(dimethylamino)propyl]carbodiimide hydrochloride (EDC), *N*-hydroxysuccinimide (NHS), diethylenetriaminepen-

DOI: 10.1021/am508118x
ACS Appl. Mater. Interfaces 2015, 7, 2847−2855

tacetate acid (DTPA), Tween20, Oil Red O, propylene glycol, sodium pentobarbital, 1,3,4,6-tetrachloro-3a,6a-diphenylglucoluril (Iodogen), COOH−PEG−COOH (M_w = 3400 Da), and COOH−PEG−NH_2 (M_w = 3400 Da). All of the above were purchased from Sigma, St. Louis, MO. Additional materials include Annexin V (Human recombinant; Abcam, Cambridge, MA), isoflurane (Baxter Healthcare, Guayama, Puerto Rico), $Na^{99m}TcO_4$ and $Na^{125}I$ (Shanghai GMS Pharmaceutical Co., Ltd., Shanghai, China), ^{18}F-FDG (Shanghai Atom Kexing Pharmaceuticals Co., Ltd., Shanghai, China), analytical phosphate-buffered saline (PBS; 0.2 M), dichloromethane, $SnCl_2{\cdot}2H_2O$, H_2O_2, and acetone, which were purchased from China National Pharmaceutical Group Corp., Beijing, China, Dulbecco's modified eagle medium (DMEM) medium (Gibco, USA, Grand Island, NY), Whatman 3MM chromatography paper (GE Healthcare UK Limited, Buckinghamshire, U.K.), aluminum-backed flexible silica thin-layer chromatography plates and a TUNEL Apoptosis Detection Kit (Merck KGaA, Darmstadt, Germany), and anti-CD68 antibody (Abcam, Cambridge, MA). ^{125}I-Annexin V was prepared in house via the Iodogen method with a radiochemical purity of >95%.[24]

A macrophage cell line (RAW264.7) was cultured in a DMEM medium with 10% fetal bovine serum and incubated in 5% CO_2 at 37 °C. Cellular apoptosis was induced via incubation with 2.5 nM H_2O_2 for 3 h. Animal care and all experimental procedures were performed under the approval of the Animal Care Committee of Fudan University. C57 mice (male, 10 weeks, weight 20−25 g each) and ApoE$^{-/-}$ mice (male, 10 weeks, weight 20−25 g each) were provided by the Peking University Laboratory Animal Center. ApoE$^{-/-}$ mice were continually fed on a high-fat diet (containing 21% fat and 0.15% cholesterol by weight) for more than 10 weeks.[25] Inclusion criteria were as follows. Every mouse fed with a high-fat diet was preevaluated by ^{18}F-FDG PET; ApoE$^{-/-}$ mice with obvious high standard uptake value in the aorta region were recruited in the study group. Normal C57 mice, which were preevaluated by ^{18}F-FDG PET as AS plaques negative, were recruited in the control group.

Fabrication and Characterization of a Dual-Modal SPECT/MRI Agent. Ultrasmall superparamagnetic iron oxide was synthesized via thermal decomposition of iron(III) acetylacetonate in diethylene glycol.[26] The synthetic schema of ^{99m}Tc−DTPA−USPIO−Annexin V is presented in Figure 1. Generally, nano-Fe_3O_4 was dissolved in 50-fold (molar ratio, similar hereinafter) COOH−PEG−NH_2- and COOH−PEG−COOH-containing PBS at 20 μg/mL. The system was then subjected to ultrasound treatment for 1 h at room temperature. The mixed solution was centrifuged at 300 g (same rate was that used in the following steps) to collect COOH−PEG−NH_2/Fe_3O_4/COOH−PEG−COOH nanomagnetofluid and remove free PEGs. In the process of functionalization, 20-fold DTPA in dimethyl suloxide was added for conjugation to −COOH. After 1 h of reaction at room temperature, the solution was centrifuged to remove free DTPA. Little Tween20, 100-fold EDC, and 25-fold NHS (compared to -NH_2) were dissolved in USPIO−DTPA-containing PBS. The final solution was oscillated for 30 min and then centrifuged to remove unattached molecules. Finally, Annexin V was added to the solution and then oscillated for 2 h at room temperature or overnight at 4 °C. DTPA−USPIO−Annexin V was finally harvested by centrifugation as well. The morphology and size of the hybrid nanoparticle system were characterized using TEM at an acceleration voltage of 200 kV; the thickness of the PEG cover was measured by dynamic light scattering; measurement of the surface ζ potential was performed by a zetasizer to evaluate the PEG cover and DTPA coupling.

Following the ^{99m}Tc-labeling method,[27] 20 μL of a NH_4OAc solution (0.25 mol/L), 20 μL of a buffer solution (0.5 mol/L $NaHCO_3$, 0.25 mol/L NH_4OAc, 0.175 mol/L NH_4OH; pH 9.2), 40 μL of $Na^{99m}TcO_4$ (37−370 MBq/mL), and 10 μL of $SnCl_2{\cdot}2H_2O$ (1 mg/mL, in 10 mM HCl) were added to 50 μL of a DTPA−USPIO−Annexin V suspension to obtain a final pH of 8.4. After 30 min of reaction at room temperature, a ^{99m}Tc−DTPA−USPIO−Annexin V solution was harvested. The labeling rate and stability in PBS and a 10% bovine serum albumin solution were measured by RTLC, using acetone as the developing solvent: ^{99m}Tc−DTPA−USPIO−Annexin V, R_f = 0; $Na^{99m}TcO_4$, R_f = 0.7. Considering the relatively short half-life period ($T_{1/2}$ = 6.0058 h) of ^{99m}Tc and the circulation of the hybrid nanoparticle system, in vitro stability was measured for 12 h at most.

In Vitro Cellular Uptake. To check the targeting ability and specificity of this hybrid nanoparticle, in vitro cellular uptake experiments of USPIO with or without Annexin V were performed. A total of 50 μg of radiolabeled USPIO (high concentration) or 5 μg of radiolabeled USPIO (low concentration) with or without Annexin V was added to 5 × 10^6 apoptotic macrophages and incubated for another 2 h. Cells were gently washed by water twice and then collected for measurement of the specific uptake.

In Vivo PET, SPECT/CT, and MRI. Before being recruited into the multimodal imaging study group, ApoE$^{-/-}$ mice were preevaluated by ^{18}F-FDG PET for confirmation of AS. Part of the ApoE$^{-/-}$ mice underwent ^{125}I-Annexin V SPECT to verify in vivo targeting effects and to monitor the pharmacokinetics, an important reference in investigating ^{99m}Tc−DTPA−USPIO−Annexin V SPECT/MRI. Because of the limitations of the current techniques, multimodal scanning was performed separately; MRI was performed 3 h after SPECT. Two radiologists first independently evaluated all four series of images below, and then a statistician performed quantitative analysis. Details are given below.

^{18}F-FDG PET. ^{18}F-FDG (7.4 MBq/mouse) was intravenously injected into all ApoE$^{-/-}$ mice and C57 mice. At 3 h after injection, mice were anesthetized via 2% isoflurane inhalation. Depending on the count rate, 20 min static PET images were acquired and then reconstructed using a two-dimensional ordered-subset expectation maximum (2D OSEM) algorithm, and no correction was applied for attenuation or scatter. Spatial resolution was 2 mm for PET imaging.

^{125}I-Annexin V SPECT/CT. ^{125}I-Annexin V (18.5 MBq/mouse) was administered to ApoE$^{-/-}$ and C57 mice via tail vein injection. At 3 h after injection, mice were anesthetized via 2% isoflurane inhalation. CT was performed with the following scan parameters: frame resolution, 256 × 512; tube voltage, 45 kVp; current, 0.15 mA; exposure time, 500 ms/frame. Each scan took about 7 min. Real-time 3D reconstruction of the collected images was performed using the *Nucline* software (v 1.02, Mediso, Budapest, Hungary). SPECT was performed after CT scanning using the following parameters: four high-resolution, conical collimators with 9-pinhole plates; energy peak, 28 keV; window width, 10%; resolution, 1 mm/pixel; matrix, 256 × 256; scan time, 60 s/projection with 24 projections in all. The whole-body scan for each mouse took 24 min on average. Three-dimensional ordered-subset expect-

DOI: 10.1021/am508118x
ACS Appl. Mater. Interfaces 2015, 7, 2847−2855

ation maximization images were reconstructed using HiSPECT (Bioscan, Washington, DC).

SPECT/CT and MRI Using a Dual-Modal Agent. ApoE$^{-/-}$ and C57 mice were administered ^{99m}Tc−DTPA−USPIO−Annexin V (18.5 MBq/mouse) via tail vein injection. As a verification of in vivo specificity, some ApoE$^{-/-}$ mice were administered ^{99m}Tc−DTPA−USPIO (18.5 MBq/mouse). Three mice per group were recruited for the following investigations. The pharmacokinetics and in vivo distribution of ^{99m}Tc−DTPA−USPIO−Annexin V in mice were monitored using micro-SPECT/CT with the same device parameters as those of ^{125}I-Annexin V SPECT/CT but an energy peak of 140 keV. For the mouse used above, MRI scanning was performed after 5 h of SPECT/CT with an interval of less than 3 h. In vivo MRI studies were performed with a 3T horizontal-bore scanner via a gradient-echo FLASH sequence: repetition time, 2000 ms; echo time, 40 ms; field of view, 75 × 100 mm^2; matrix, 192 × 256; thickness of each slice, 2 mm; with no gaps. A dedicated mouse cardiac volume coil was used, and mice were anesthetized via intraperitoneal injection of 100 μL of 4% sodium pentobarbital. For biodistribution analysis, ID%/mm^3 was obtained by using InVivoScope 1.4 (Bioscan, Washington, DC) to outline the organs, including heart, lung, liver, kidneys, spleen, and intestine on SPECT images at 2, 5, and 12 h. Blood samples were continuously collected during the first 12 h postinjection for measurement of the blood clearance. All data were decay-corrected to the injection time.

Ex Vivo Planar Imaging of the Aorta. In order to further eliminate potential confounding factors such as mismatch and low positive value led by a low-signal intensity, BSGI was used for ex vivo planar images of the dissected aorta. ^{99m}Tc−DTPA−USPIO−Annexin V (18.5 MBq/mouse) was administered to ApoE$^{-/-}$ and C57 mice (different from the ones recruited in in vivo imaging) via tail vein injection. Mice were anesthetized and then sacrificed at 5 or 24 h after injection for ex vivo planar imaging of the aorta. A total of 5 mL of 0.9% NaCl and 5 mL of 4% paraformaldehyde were orderly and slowly injected in the blood system to eject the blood and fix the vessels. The aorta was carefully and completely dissected from the body and then placed in the central position of the BSGI camera for planar imaging with the following parameters: high-resolution collimator; collecting peak energy, 140 keV; window width, 10%; resolution, 0.32 mm/pixel; matrix, 80 × 80. The collection time was 5−10 min with total collection counts of 80000−100000.

In Vitro Histological Studies. In order to verify that ^{125}I-Annexin V accumulations in the aortas of mice are because of specific targeting to apoptotic macrophages, in vitro histological studies were further conducted after imaging. CD-68 staining was used to evaluate the macrophages by staining cell nuclei, and the TUNEL technique was used to distinguish the apoptotic cells with fragmented DNA. ApoE$^{-/-}$ mice that experienced ^{125}I-Annexin V SPECT/CT examinations were sacrificed for immunohistochemical experiments, in which their aortas relevant to high SPECT signal were paraffin-embedded and sliced. The adjacent three slices were selected for hematoxylin and eosin staining, CD-68 staining, and TUNEL staining, respectively, following the manufacturer's protocols on the commercial staining kits.

For mice recruited into the ^{99m}Tc−DTPA−USPIO−Annexin V SPECT/MRI imaging group, Oil Red O was used to stain lipid deposits inside atherosclerotic lesions. Variation in Oil Red O staining allowed us to stratify the lesions into those with high or low lipid content, which indirectly indicated the vulnerability of AS plaques.[12] The dissected aorta was air-dried for 30−60 min at room temperature and then fixed in ice-cold 10% formalin for 5−10 min. The fixed aorta was placed in absolute propylene glycol for 5 min to avoid carrying water into Oil Red O. Staining in a prewarmed 0.5% Oil Red O solution (in propylene glycol) lasted for 30 min. Finally, the aorta was differentiated in a 85% propylene glycol solution for 5 min: Lipids were stained as red, while nuclei were pale blue. Following the reported methodology,[12] the intensity of staining was further graded from 0 to 3 (where 0 means not stained, 1 means slightly stained, 2 means intensively stained, and 3 means very intensively stained).

Statistics. Statistical analysis was carried out using *SPSS 19.0*. Any results with a p value <0.05 were considered as statistically significant. In order to investigate the correlation between dual-modal images and vulnerability, four typical regions with Oil Red O staining scores of 0, 1, 2, and 3 were selected; linear regression analyses were performed on the corresponding signal intensity of SPECT and planar images and the signal change of MR images.

RESULTS AND DISCUSSION

Fabrication of a Dual-Modal SPECT/MRI Probe. The as-synthesized water-soluble ultrasmall iron oxide nanoparticles were monodispersed with a uniform size of 3−5 nm, as stated via TEM images (Figure 2a). At room temperature, these

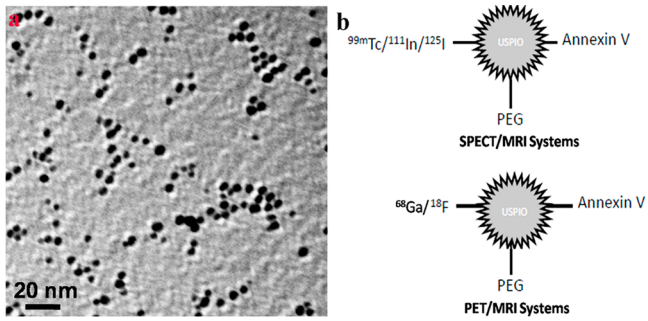

Figure 2. TEM image of USPIO used in this research (a) and the potential usage of a USPIO-based hybrid nanoparticle system as SPECT/MR and PET/MRI probes (b).

Fe_3O_4 behaved superparamagnetically (i.e., no hysteresis and immeasurable coercivity and remanence exhibited). USPIO was fully covered with equal NH_2−PEG−COOH and COOH−PEG−COOH, as demonstrated by the electric neutrality of a harvested magnetofluid. A ∼20 nm shell of PEGs formed on the surface and provided equal −NH_2 and −COOH groups for DTPA coupling and Annexin V coupling. When the amounts of NH_2−PEG−COOH and COOH−PEG−COOH were changed, the corresponding ratio of targeting molecules and ^{99m}Tc could be adjusted, but this was not the research emphasis in this study. The electric neutrality of a COOH−PEG−NH_2/Fe_3O_4/COOH−PEG−COOH nanomagnetofluid and Annexin V−USPIO indicated the successful grafting of molecules, a precondition of radiolabeling, and stability of the hybrid nanoparticle system.

Normally, 37 MBq $^{99m}TcO_4^-$ corresponded to 1 μg of $SnCl_2\cdot 2H_2O$, with a primary labeling rate of >97% after 1 h of reaction. Hence, no further purifying steps were needed. In the saturation test, the maximum of labeled radioactivity was 370

DOI: 10.1021/am508118x
ACS Appl. Mater. Interfaces 2015, 7, 2847−2855

MBq for 1 mg of USPIO. More than 95% of ^{99m}Tc remained on USPIO during the first 6 h, whether in PBS or 10% serum. The radiochemical purity decreased to about 90% by 12 h because of the breakdown of weak covalent coordination bonds and the nonspecific bonding to Annexin V. In the final products, 10 μg of Annexin V normally corresponded to 1 mg of iron and 18.5 MBq radioactivity in 200 μL injection. The transverse (r_2) and longitudinal (r_1) relaxivities of ^{99m}Tc−DTPA−USPIO−Annexin V were around 20.1 and 8.2 $s^{-1}mM^{-1}$, with r_2/r_1 = 2.5.

Synthesis of this hybrid nanoparticle system is based on the general scheme of constructing multiple functional agents, providing the potential for combining other imaging nuclide and target molecules. As stated in this research, the nanoparticle platform was usually modified with abundant $-NH_2$ or −COOH groups, which provided the dehydration reaction sites for conjugation of functional molecules. Lots of NHS-based biolinkers, such as EDC/NHS, AMAS, BMPS, and SMCC, were developed for immobilization of protein$-NH_2$, protein−SH, and so on to nanoparticles$-NH_2$.[28,29] For radiolabeling, DTPA and analogues were widely used for metal nuclide chelating, such as ^{111}In, ^{153}Sm, etc.,[30−35] because of the convenient reaction process and high labeling efficiency. BTAP, EC, NHS−MAG_3, and HYNIC were also utilized for chelating ^{99m}Tc to Annexin V with a high labeling rate: normally >90%, even 95% for ^{99m}Tc−Annexin V.[30] Similarly, ^{18}F and ^{68}Ga were also able to label the hybrid nanoparticle system, taking advantage of the superior characteristics of PET.[19] In brief, the items above make this system potentially applicable for both SPECT/MRI and PET/MRI with flexibility for a variety of isotope labeling. Another benefit is that targeting effects and specificity can be adjusted by replacing the target molecules.

Targeting Specificity for Vulnerable Plaques. The high-fat-fed spontaneous AS in the ApoE$^{-/-}$ mice models was proven to develop slowly in the aortic tissues throughout the arterial tree and had a relatively low success rate.[36,37] In the in vivo specificity test, ^{125}I-Annexin V was selected considering the relatively long radioactive $T_{1/2}$ of radionuclide and the convenient synthesis route. Notably, absorption of ^{125}I-Annexin V was roughly the same with ^{18}F-FDG, in agreement with Zhao's conclusions that both ^{99m}Tc-Annexin V and ^{18}F-FDG showed preferential uptake in AS lesions.[12] The advanced lesions confirmed by ^{18}F-FDG PET and ^{125}I-Annexin V SPECT were predominantly located in the ascending aorta and in the abdominal aorta. However, ^{125}I-Annexin V was more concentrated and exhibited a higher ratio of lesions to background (Figure 3c,d). Meanwhile, there was no obvious accumulation of probes in the aorta of C57 mice.

In immunohistochemistry tests, the existence of macrophages in the highlighted lesions was confirmed by the abundantly stained cell nuclei of the thoracic and abdominal aorta in the CD-68 stained plaques (Figure 3f,i) and further confirmed as apoptotic cells by the TUNEL technique (Figure 3g,j). Furthermore, the more severe lesions associated with a higher ratio of CD-68 and TUNEL stained cells were displayed in the ascending aorta, where a more intense radioactive signal was shown as well. Consequently, both in vivo and in vitro results confirmed the specificity of Annexin V as a target molecule in targeting vulnerable plaques containing apoptotic macrophages. The target efficiency was proportional to the vulnerability of AS plaques.

The specificity of Annexin V−USPIO was also proven via in vitro cellular uptake and in vivo lesional uptake. There was a

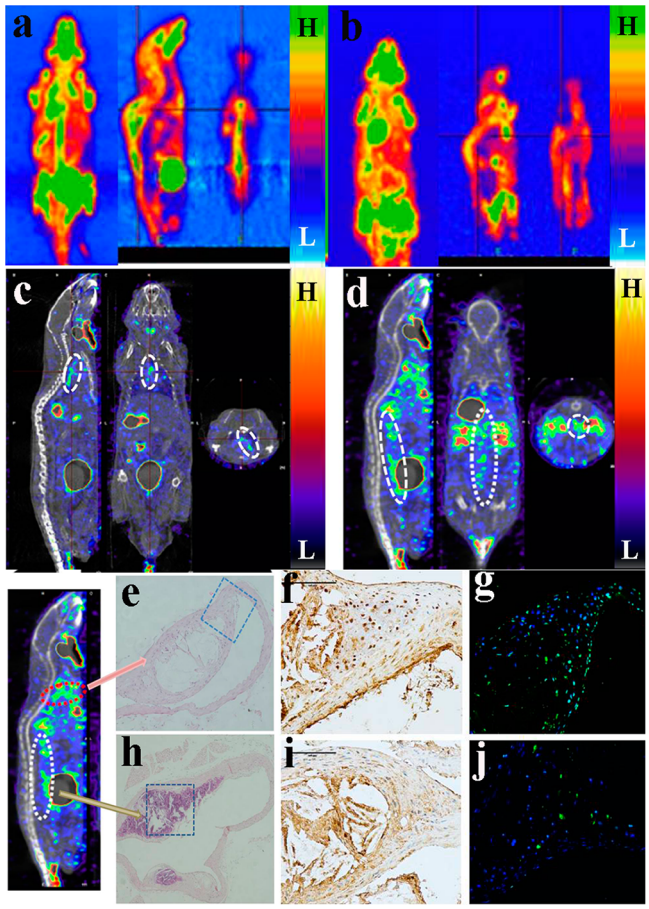

Figure 3. Two typical ^{18}F-FDG PET images of ApoE$^{-/-}$ mice (a) and C57 mice (b) at 3 h after injection exhibited in perspective, maximum intensity projection, sagittal, and coronal views (left to right). In the ^{125}I-Annexin V SPECT/CT images (sagittal, coronal, and transverse views, left to right), probes obviously accumulated in the thoracic aorta (c) and abdominal aorta (d). The highlighted plaques in D distributed along the spinal column and ended at the kidney, consistent with the anatomical structures. Hematoxylin and eosin staining and CD-68 and TUNEL staining of the ascending aorta (e−g) and abdominal aorta (h−j) of ApoE$^{-/-}$ mice are also shown here; corresponding positions are circled in the ^{125}I-Annexin V SPECT/CT images. "H" means high signal, and "L" means low signal (similarly hereinafter).

significant increase of specific cellular uptake after Annexin V conjugation when a modest amount of USPIO was used. Similarly, there was a relatively higher level of the ^{99m}Tc−USPIO−Annexin V signal compared with that of ^{99m}Tc−USPIO. Hence, Annexin V made the hybrid nanoparticle apoptotic macrophage targeted in vitro and vulnerable plaques targeted in vivo. Comparisons between Annexin V−USPIO and USPIO for cellular and lesional uptake are pictured in Figure 4.

SPECT/MRI of Vulnerable AS Plaques. Compared with ^{125}I-Annexin V SPECT/CT, the most obvious change of the ^{99m}Tc−DTPA−USPIO−Annexin V SPECT images was the abundant accumulation of radioactivity in reticuloendothelial system (RES)-related organs, especially the lung and liver. The significant signal from AS plaques can be observed at 5 h postinjection, accompanied by an increase of the signal from the liver, lung, and bladder, as well as during the first 5 h. However, the contrast of AS plaques to adjacent normal tissues was adequate for AS plaque differentiation. Although the best imaging period after injection was prolonged to 5 h, the

DOI: 10.1021/am508118x
ACS Appl. Mater. Interfaces 2015, 7, 2847−2855

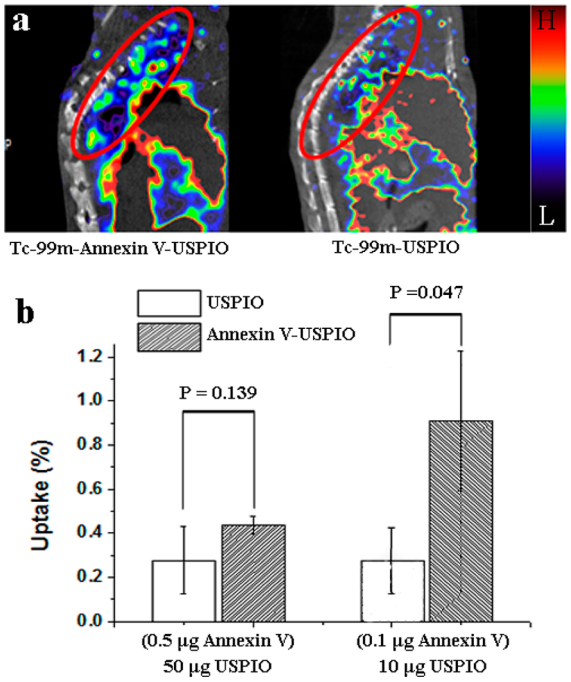

Figure 4. Comparisons between Annexin V−USPIO and USPIO for cellular and lesional uptake. For the in vivo comparison (a), lesions are outlined in the red circle. For the in vitro comparisons (b), the significance levels are marked on top of the columns.

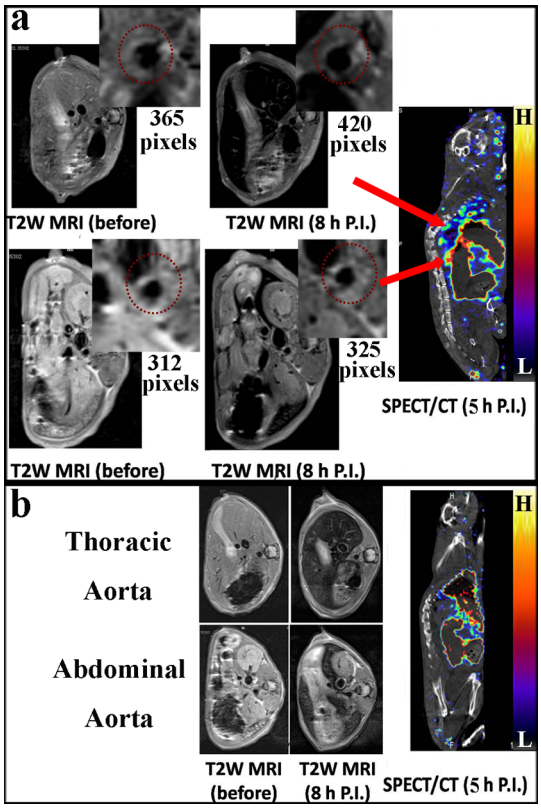

Figure 5. In vivo SPECT/MRI images of ^{99m}Tc−DTPA−USPIO−Annexin V in ApoE$^{-/-}$ mice and C57 mice. For SPECT images, AS plaques were clearly seen in the thoracic and abdominal aorta (a) but not seen in the similar region of C57 mice (b). In both models, abundant radioactivity accumulated in the lung and liver. For MR images, the transverse series of AS plaques are shown. The T2 signal (8 h postinjection) in the circled thoracic and abdominal aorta was lower than the T2 signal before injection for ApoE$^{-/-}$ mice (a). However, this change of the T2 signal in the aorta region was not observed in C57 mice (b). The involved pixels of AS plaques in the transverse image are shown as well, indicating the possibility of plaques volumetry.

specificity for vulnerable plaques was still exhibited. In contrast, the aorta of the control C57 mouse exhibited no obvious absorption of ^{99m}Tc−DTPA−USPIO−Annexin V after injection (Figure 5b). However, the massive accumulation of particles in RESs was the same as that for ApoE$^{-/-}$ mice, confirming the lack of abundant apoptotic cells in the aorta of control C57 mice.

For ^{99m}Tc−DTPA−USPIO−Annexin V T2MRI, the obvious signal change of AS plaques can be observed at 8 h postinjection. Signals from RESs and AS plaques decreased notably because of absorption of USPIO, leading to a "dark" view. Similar to the lung and liver, absorption of USPIO by apoptotic macrophages decreased the T2 signal of AS plaques in the aorta, enhancing the contrast of lesion to normal tissues, especially for the aorta, where the region with normal blood is exhibited as "absolute dark". Upon integration with the MR images taken before the injection, lesions in the aorta can be clearly outlined manually, facilitating the localization and volumetry of AS plaques. The involved scope and extent of AS plaques in vessels can be clearly described, as shown as the involved pixels in Figure 4. Similar to the SPECT images, changes in the aortic region of C57 mice were not observed (Figure 5b) because of the lack of apoptotic cells.

As a multimodal imaging probe for SPECT/MRI, radionuclide and USPIO should be balanced and considered as a whole, although SPECT and MRI investigations were performed separately in this study. The radioactivity used in this research was 18.5 MBq, fulfilling the usual radioactivity requirement for a SPECT/CT scan. The weight of USPIO injected was 1 mg/mouse (at the micromolar scale), a higher amount than that used in in vitro cellular imaging,[20] considering the fact that part of the nanoparticles will be captured by the RES before attachment to the target. Herein, the radioactivity for SPECT imaging and the chemical amount of USPIO for T2-weighted MRI can be adjusted for a balanced SPECT/MRI view. As mentioned above, the final ratio of ^{99m}Tc to USPIO was fixed to 18.5 MBq/mg (10 μg of Annexin V contained), an appropriate choice for SPECT/MRI. This dosage was based on the specific equipment used in this study. A more sensitive radiodetector or a higher field strength would decrease the needed radioactivity or chemical amount of USPIO. The details of biodistribution (Figure 6) were consistent with imaging results. The imaging agent quickly targeted plaques and accumulated in RES-related organs. The target to nontarget ratio increased as the agent was gradually expelled from RES-related organs, but the agent remained in lesions for a longer period.

These results support the feasibility of simultaneous SPECT/MRI via a single ^{99m}Tc−DTPA−USPIO−Annexin V probe. Benefits from integrated imaging include the enhanced reliability of focal localization and increased contrast between lesion and normal tissues. As an investigation of feasibility, little effort has been put forth to optimize the imaging parameters, such as the dosage and imaging periods. Nonetheless, we can conclude for now that 5 h postinjection can fulfill the requirement of the circulation period of this SPECT/MRI

DOI: 10.1021/am508118x
ACS Appl. Mater. Interfaces 2015, 7, 2847−2855

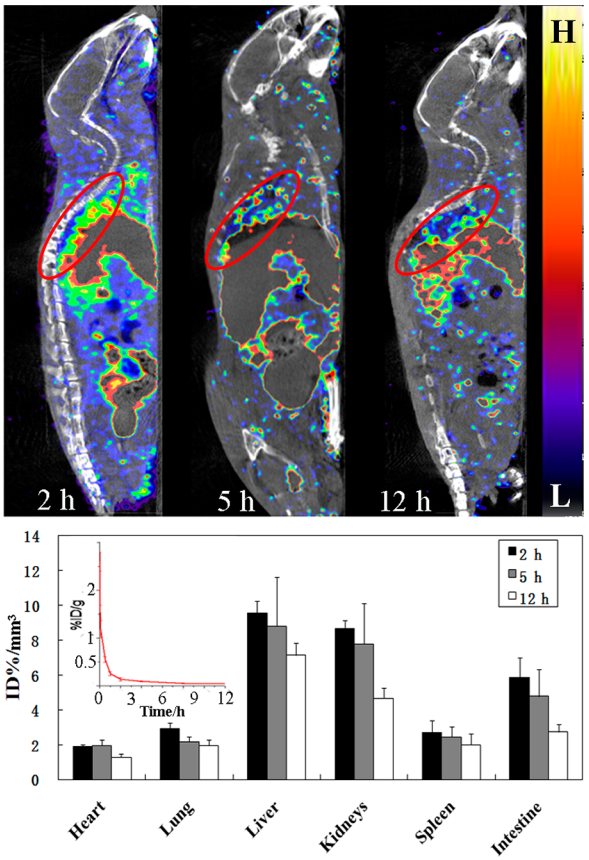

Figure 6. Biodistribution of ^{99m}Tc−USPIO−Annexin V at 2, 5, and 12 h. The blood clearance tendency is plotted as well (red line).

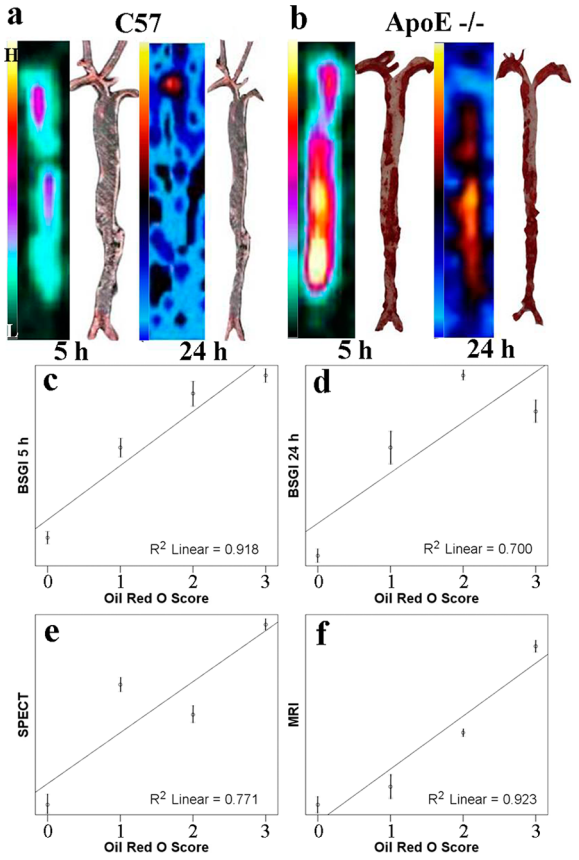

Figure 7. Set of 5 and 24 h BSGI images and the corresponding Oil Red O staining results for C57 mice (a) and ApoE$^{-/-}$ mice (b). The 24 h BSGI images of other mice are shown for reference. The linear relationship of the SPECT signal, MRI signal, BSGI signal, and Oil Red O staining scores are depicted in parts c−f, where the relative value of the image signal was used for a better view.

probe. This proposal is further confirmed by ex vivo planar images, which will be discussed later.

Ex Vivo Confirmation of SPECT/MR Image Results. The planar view of the radioactivity distribution is a direct reflection of AS plaques and more closely corresponds to vulnerability. Furthermore, by use of this planar imaging modality, the signal-to-noise ratio could be enhanced to accurately recognize small foci with low uptake, avoiding interference from the surrounding tissue with high radioactivity accumulation (Figure 7a,b). In planar images, radioactivity distributed along the whole aorta of ApoE$^{-/-}$ mice but most intensely in the aortic root, aortic arch, and abdominal aorta. Occasional lesions besides these two common regions were also easily found based on the BSGI. It is interesting to note that no obvious accumulation of radioactivity was observed in planar aorta images of C57 mice but in the aortic arches; a similar situation was observed in the ^{125}I-Annexin V SPECT/CT images. Lesions in the aortic arch of C57 mice may result from the relatively long life span of these model mice, which is a main reason for AS development. The distribution of radioactivity reflected by planar imaging in Figure 7b was similar to the distribution of ^{99m}Tc−DTPA−USPIO−Annexin V in Figure 5a but not totally the same. This may result from the progressive property of AS plaques or interference from the higher load of probes by adjacent organs.

Poor clearance of apoptotic macrophages may lead to the accumulation of cellular debris within the lipid-rich core of atherosclerotic plaque; thus, lipid-related Oil Red O staining reflects the amount of apoptotic macrophages, as well as the vulnerability of AS plaques.[30] Oil Red O staining of the aorta can totally reproduce the SPECT/MRI and BSGI images, such as those shown in Figure 7a,b. Lesions with high radioactivity normally correspond to a high score in Oil Red O staining. Linear regression further clarified the relationship between the SPECT/MRI and lesions and between planar images and lesions. The linear relationships between the SPECT signal and Oil Red O staining, MRI signal change and Oil Red O staining, 5 h BSGI signal and Oil Red O, and 24 h BSGI signal and Oil Red O were all statistically significant, with R^2 values of 0.771, 0.923, 0.918, and 0.7, respectively. Therefore, 5 h was a better choice than 24 h in imaging the lesions. Currently, it is difficult to quantify plaques with small size solely using nuclear medicine imaging modality because of partial volume effects. Therefore, this hybrid SPECT/MRI probe provides the possibility of differentiating vulnerable plaques from stable plaques by virtue of an accurate quantification function via the combination of quantification characterization of SPECT and soft-tissue-recognition ability of MRI.

Safety and Application Prospect. As a commonly used protein specifically targeted to apoptotic cells, Annexin V-based agents have been conducted through extensive studies in hybrid optical imaging and MRI for cancer diagnosis.[38,39] Moreover, Annexin V has been investigated as a bimodal imaging probe for MRI and fluorescence imaging of AS plaques, but both modalities are oriented to achieve high-resolution images.[40] However, in this study, Annexin V was for the first time conjugated with radiolabeled USPIO as a SPECT/MRI

DOI: 10.1021/am508118x
ACS Appl. Mater. Interfaces 2015, 7, 2847−2855

bimodal imaging probe. Herein, high sensitivity and quantifiability can be realized by SPECT, and high resolution and soft tissue contrast can be achieved by MRI. On the basis of a long period of observation, injections was deemed safe for mice; no noticeable physiological or behavioral abnormalities were detected weeks after vein injection. The major limitation of this study is the separate investigations of ^{99m}Tc−DTPA−USPIO−Annexin V SPECT and MRI, which hampered the simultaneous image acquisition and subsequent image fusing. However, separate imaging will not be an obstacle for usage of this hybrid nanoparticle-based dual-modal imaging agent. Some efforts on theory and practice have been made for dual-modal PET/MRI, especially for cerebral and cardiovascular imaging, and some encouraging clinical outcomes have been reported.[41,42] A lot of benefits, such as reducing radiation and the combination of high resolution and high sensitivity, have proven the necessity of its popularization and application. Hence, this research on dual-modal imaging agent can contribute to the development of dual-modal imaging, as well as vulnerable AS plaque diagnosis.

CONCLUSION

The USPIO-based hybrid nanoparticle system was successfully fabricated, and targeting was realized via the conjugation of Annexin V. ^{99m}Tc was labeled to the particles with a labeling rate of >97% and with fine in vitro stability. This hybrid nanoparticle system may be applicable to more diseases as a targeting imaging probe in PET/MRI or SPECT/MRI.

Upon imaging of ApoE$^{-/-}$ mice, targeting for the vulnerable AS plaques of ^{99m}Tc−DTPA−USPIO−Annexin V as reflected by SPECT/CT and MRI was remarkably consistent. SPECT/MRI using ^{99m}Tc−DTPA−USPIO−Annexin V provided more information on localizing and identifying vulnerable plaques. The higher uptake levels of ^{99m}Tc−DTPA−USPIO−Annexin V in macrophages indicate the potential ability of this agent to identify apoptosis with a higher risk of rupture, and the precise outline of lesions makes this method helpful for volumetry.

AUTHOR INFORMATION

Corresponding Author

*E-mail: shi.hongcheng@zs-hospital.sh.cn. Tel: +86 21 64041990-2064. Fax: +86 21 64038472.

Author Contributions

D.C. and X.L. contributed equally to this work.

Notes

The authors declare no competing financial interest.

ACKNOWLEDGMENTS

The authors thank the Fudan University Shanghai Cancer Center and East China Normal University for providing SPECT/CT and MRI service and technical assistance. This work was funded, in part, by the National Natural Science Foundation of China (Grants 81271608 and 81201130) and the Shanghai Pujiang Program (No. 13PJ1401400).

REFERENCES

(1) Lee, W. W.; Marinelli, B.; van der Laan, A. M.; Sena, B. F.; Gorbatov, R.; Leuschner, F.; Dutta, P.; Iwamoto, Y.; Ueno, T.; Begieneman, M. P. V; Niessen, H. W. M.; Piek, J. J.; Vinegoni, C.; Pittet, M. J.; Swirski, F. K.; Tawakol, A.; Di Carli, M.; Weissleder, R.; Nahrendorf, M. PET/MRI of Inflammation in Myocardial Infarction. *J. Am. Coll. Cardiol.* **2012**, *59*, 153−163.

(2) Xing, H.; Bu, W.; Zhang, S.; Zheng, X.; Li, M.; Chen, F.; He, Q.; Zhou, L.; Peng, W.; Hua, Y.; Shi, J. Multifunctional Nanoprobes for Upconversion Fluorescence, MR and CT Trimodal Imaging. *Biomaterials* **2012**, *33*, 1079−1089.

(3) Ni, D.; Zhang, J.; Bu, W.; Xing, H.; Han, F.; Xiao, Q.; Yao, Z.; Chen, F.; He, Q.; Liu, J.; Zhang, S.; Fan, W.; Zhou, L.; Peng, W.; Shi, J. Dual-targeting Upconversion Nanoprobes across the Blood-brain Barrier for Magnetic Resonance/Fluorescence Imaging of Intracranial Glioblastoma. *ACS Nano* **2014**, *8*, 1231−1242.

(4) Xing, H.; Zhang, S.; Bu, W.; Zheng, X.; Wang, L.; Xiao, Q.; Ni, D.; Zhang, J.; Zhou, L.; Peng, W.; Zhao, K.; Hua, Y.; Shi, J. Ultrasmall $NaGdF_4$ Nanodots for Efficient MR Angiography and Atherosclerotic Plaque Imaging. *Adv. Mater.* **2014**, *26*, 3867−3872.

(5) Ishino, S.; Mukai, T.; Kuge, Y.; Kume, N.; Ogawa, M.; Takai, N.; Kamihashi, J.; Shiomi, M.; Minami, M.; Kita, T.; Saji, H. Targeting of Lectinlike Oxidized Low-density Lipoprotein Receptor 1 (LOX-1) with ^{99m}Tc-labeled Anti-LOX-1 Antibody: Potential Agent for Imaging of Vulnerable Plaque. *J. Nucl. Med.* **2008**, *49*, 1677−1685.

(6) Li, D.; Patel, A. R.; Klibanov, A. L.; Kramer, C. M.; Ruiz, M.; Kang, B.-Y.; Mehta, J. L.; Beller, G. a; Glover, D. K.; Meyer, C. H. Molecular Imaging of Atherosclerotic Plaques Targeted to Oxidized LDL Receptor LOX-1 by SPECT/CT and Magnetic Resonance. *Circ. Cardiovasc. Imaging* **2010**, *3*, 464−472.

(7) Rudd, J. H. F.; Hyafil, F.; Fayad, Z. A. Inflammation Imaging in Atherosclerosis. *Arterioscler. Thromb. Vasc. Biol.* **2009**, *29*, 1009−1016.

(8) Zhang, Y.-R.; Zhang, Y.-X.; Cao, W.; Lan, X.-L. Uptake Kinetics of ^{99m}Tc-MAG_3-antisense Oligonucleotide to PCNA and Effect on Gene Expression in Vascular Smooth Muscle Cells. *J. Nucl. Med.* **2005**, *46*, 1052−1058.

(9) Kolodgie, F. D.; Petrov, A.; Virmani, R.; Narula, N.; Verjans, J. W.; Weber, D. K.; Hartung, D.; Steinmetz, N.; Vanderheyden, J. L.; Vannan, M. A.; Gold, H. K.; Reutelingsperger, C. P. M.; Hofstra, L.; Narula, J. Targeting of Apoptotic Macrophages and Experimental Atheroma with Radiolabeled Annexin V: a Technique with Potential for Noninvasive Imaging of Vulnerable Plaque. *Circulation* **2003**, *108*, 3134−3139.

(10) Britz-Cunningham, S. H.; Adelstein, S. J. Molecular Targeting with Radionuclides: State of the Science. *J. Nucl. Med.* **2003**, *44*, 1945−1961.

(11) Kemerink, G. J.; Liu, X.; Kieffer, D.; Ceyssens, S.; Mortelmans, L.; Verbruggen, A. M.; Steinmetz, N. D.; Vanderheyden, J.-L.; Green, A. M.; Verbeke, K. Safety, Biodistribution, and Dosimetry of ^{99m}Tc-HYNIC-Annexin V, a Novel Human Recombinant Annexin V for Human Application. *J. Nucl. Med.* **2003**, *44*, 947−952.

(12) Zhao, Y.; Kuge, Y.; Zhao, S.; Morita, K.; Inubushi, M.; Strauss, H. W.; Blankenberg, F. G.; Tamaki, N. Comparison of ^{99m}Tc-annexin A5 with ^{18}F-FDG for the Detection of Atherosclerosis in ApoE$^{-/-}$ mice. *Eur. J. Nucl. Med. Mol. Imaging* **2007**, *34*, 1747−1755.

(13) Boersma, H. H.; Kietselaer, B. L. J. H.; Stolk, L. M. L.; Bennaghmouch, A.; Hofstra, L.; Narula, J.; Heidendal, G. a. K.; Reutelingsperger, C. P. M. Past, Present, and Future of Annexin A5: from Protein Discovery to Clinical Applications. *J. Nucl. Med.* **2005**, *46*, 2035−2050.

(14) Ito, A.; Shinkai, M.; Honda, H.; Kobayashi, T. Medical Application of Functionalized Magnetic Nanoparticles. *J. Biosci. Bioeng.* **2005**, *100*, 1−11.

(15) Hao, R.; Xing, R.; Xu, Z.; Hou, Y.; Gao, S.; Sun, S. Synthesis, Functionalization, and Biomedical Applications of Multifunctional Magnetic Nanoparticles. *Adv. Mater.* **2010**, *22*, 2729−2742.

(16) He, W.; Cheng, L.; Zhang, L.; Liu, Z.; Cheng, Z.; Zhu, X. Facile Fabrication of Biocompatible and Tunable Multifunctional Nanomaterials via Iron-mediated Atom Transfer Radical Polymerization with Activators Generated by Electron Transfer. *ACS Appl. Mater. Interfaces* **2013**, *5*, 9663−9669.

(17) Figge, L.; Appler, F.; Chen, H. H.; Sosnovik, D. E.; Schnorr, J.; Seitz, O.; Taupitz, M.; Hamm, B.; Schellenberger, E. Direct Coupling of Annexin A5 to VSOP Yields Small, Protein-covered Nanoprobes for MR Imaging of Apoptosis. *Contrast Media Mol. Imaging* **2014**, *9*, 291−299.

DOI: 10.1021/am508118x
ACS Appl. Mater. Interfaces 2015, 7, 2847−2855

(18) Dash, R.; Chung, J.; Chan, T.; Yamada, M.; Barral, J.; Nishimura, D.; Yang, P. C.; Simpson, P. C. A Molecular MRI Probe to Detect Treatment of Cardiac Apoptosis In Vivo. *Magn. Reson. Med.* **2011**, *66*, 1152−1162.
(19) Van Tilborg, G. A. F.; Mulder, W. J. M.; Deckers, N.; Storm, G.; Reutelingsperger, C. P. M.; Strijkers, G. J.; Nicolay, K. Annexin A5-functionalized Bimodal Lipid-based Contrast Agents for the Detection of Apoptosis. *Bioconjugate Chem.* **2006**, *17*, 741−749.
(20) Schellenberger, E. A.; Bogdanov, A.; Högemann, D.; Tait, J.; Weissleder, R.; Josephson, L. Annexin V-CLIO: a Nanoparticle for Detecting Apoptosis by MRI. *Mol. Imaging* **2002**, *1*, 102−107.
(21) Torres Martin de Rosales, R.; Tavaré, R.; Glaria, A.; Varma, G.; Protti, A.; Blower, P. J. ^{99m}Tc-bisphosphonate-iron Oxide Nanoparticle Conjugates for Dual-modality Biomedical Imaging. *Bioconjugate Chem.* **2011**, *22*, 455−465.
(22) Chen, T.-J.; Cheng, T.-H.; Hung, Y.-C.; Lin, K.-T.; Liu, G.-C.; Wang, Y.-M. Targeted Folic Acid-PEG Nanoparticles for Noninvasive Imaging of Folate Receptor by MRI. *J. Biomed. Mater. Res., Part A* **2008**, *87*, 165−175.
(23) Lee, H.-Y.; Li, Z.; Chen, K.; Hsu, A. R.; Xu, C.; Xie, J.; Sun, S.; Chen, X. PET/MRI Dual-modality Tumor Imaging using Arginine−glycine−aspartic (RGD)-conjugated Radiolabeled Iron Oxide Nanoparticles. *J. Nucl. Med.* **2008**, *49*, 1371−1379.
(24) Lijnen, H. R.; Stassen, J. M.; Vanlinthout, I.; Fukao, H.; Okada, K.; Matsuo, O.; Collen, D. Comparative Fibrinolytic Properties of Staphylokinase and Streptokinase in Animal Models of Venous Thrombosis. *Thromb. Haemostasis* **1991**, *66*, 468−473.
(25) Hans, C. P.; Zerfaoui, M.; Naura, A. S.; Troxclair, D.; Strong, J. P.; Matrougui, K.; Boulares, A. H. Thieno[2,3-*c*]isoquinolin-5-one, a Potent Poly(ADP-ribose) Polymerase Inhibitor, Promotes Atherosclerotic Plaque Regression in High-fat Diet-fed Apolipoprotein E-deficient Mice: Effects on Inflammatory Markers and Lipid Content. *J. Pharmacol. Exp. Ther.* **2009**, *329*, 150−158.
(26) Zhang, Y.; Yang, Y.; Cai, W. Multimodality Imaging of Integrin $\alpha_v\beta_3$ Expression. *Theranostics* **2011**, *1*, 135−148.
(27) Rusckowski, M.; Qu, T.; Gupta, S.; Ley, A.; Hnatowich, D. J. A Comparison in Monkeys of ^{99m}Tc Labeled to a Peptide by 4 Methods. *J. Nucl. Med.* **2001**, *42*, 1870−1877.
(28) Mattson, G.; Conklin, E.; Desai, S.; Nielander, G.; Savage, M. D.; Morgensen, S. A Practical Approach to Crosslinking. *Mol. Biol. Rep.* **1993**, *17*, 167−183.
(29) Brinkley, M. A Brief Survey of Methods for Preparing Protein Conjugates with Dyes, Haptens, and Cross-linking Reagents. *Bioconjugate Chem.* **1992**, *3*, 2−13.
(30) Lahorte, C. M. M.; Vanderheyden, J.-L.; Steinmetz, N.; Van de Wiele, C.; Dierckx, R. A.; Slegers, G. Apoptosis-Detecting Radioligands: Current State of the Art and Future Perspectives. *Eur. J. Nucl. Med. Mol. Imaging* **2004**, *31*, 887−919.
(31) Winnard, P.; Chang, F.; Rusckowski, M.; Mardirossian, G.; Hnatowich, D. J. Preparation and Use of NHS-MAG_3 for Technetium-99m Labeling of DNA. *Nucl. Med. Biol.* **1997**, *24*, 425−432.
(32) Abrams, M. J.; Juweid, M.; TenKate, C. I.; Schwartz, D. A.; Hauser, M. M.; Gaul, F. E.; Fuccello, A. J.; Rubin, R. H.; Strauss, H. W.; Fischman, A. J. Technetium-99m-human Polyclonal IgG Radiolabeled via the Hydrazino Nicotinamide Derivative for Imaging Focal Sites of Infection in Rats. *J. Nucl. Med.* **1990**, *31*, 2022−2028.
(33) Vanderheyden, J.-L.; Liu, G.; He, J.; Patel, B.; Tait, J. F.; Hnatowich, D. J. Evaluation of ^{99m}Tc-MAG_3-annexin V: Influence of the Chelate on In Vitro and In Vivo Properties in Mice. *Nucl. Med. Biol.* **2006**, *33*, 135−144.
(34) Subbarayan, M.; Häfeli, U. O.; Feyes, D. K.; Unnithan, J.; Emancipator, S. N.; Mukhtar, H. A Simplified Method for Preparation of ^{99m}Tc-annexin V and its Biologic Evaluation for In Vivo Imaging of Apoptosis after Photodynamic Therapy. *J. Nucl. Med.* **2003**, *44*, 650−656.
(35) Grierson, J. R.; Yagle, K. J.; Eary, J. F.; Tait, J. F.; Gibson, D. F.; Lewellen, B.; Link, J. M.; Krohn, K. A. Production of [F-18]fluoroannexin for Imaging Apoptosis with PET. *Bioconjugate Chem.* **2004**, *15*, 373−379.
(36) Williams, H. Characteristics of Intact and Ruptured Atherosclerotic Plaques in Brachiocephalic Arteries of Apolipoprotein E Knockout Mice. *Arterioscler. Thromb. Vasc. Biol.* **2002**, *22*, 788−792.
(37) Coleman, R.; Hayek, T.; Keidar, S.; Aviram, M. A Mouse Model for Human Atherosclerosis: Long-term Histopathological Study of Lesion Development in the Aortic Arch of Apolipoprotein E-deficient (E0) Mice. *Acta Histochem.* **2006**, *108*, 415−424.
(38) Schellenberger, E. A.; Sosnovik, D.; Weissleder, R.; Josephson, L. Magneto/Optical Annexin V, a Multimodal Protein. *Bioconjugate Chem.* **2004**, *15*, 1062−1067.
(39) Van Tilborg, G. A. F.; Mulder, W. J. M.; Chin, P. T. K.; Storm, G.; Reutelingsperger, C. P.; Nicolay, K.; Strijkers, G. J. Annexin A5-conjugated Quantum Dots with a Paramagnetic Lipidic Coating for the Multimodal Detection of Apoptotic Cells. *Bioconjugate Chem.* **2006**, *17*, 865−868.
(40) Van Tilborg, G. A. F.; Vucic, E.; Strijkers, G. J.; Cormode, D. P.; Mani, V.; Skajaa, T.; Reutelingsperger, C. P. M.; Fayad, Z. A.; Mulder, W. J. M.; Nicolay, K. Annexin A5-functionalized Bimodal Nanoparticles for MRI and Fluorescence Imaging of Atherosclerotic Plaques. *Bioconjugate Chem.* **2010**, *21*, 1794−1803.
(41) Judenhofer, M. S.; Cherry, S. R. Applications for Preclinical PET/MRI. *Semin. Nucl. Med.* **2013**, *43*, 19−29.
(42) Nensa, F.; Schlosser, T. Cardiovascular Hybrid Imaging using PET/MRI. *RoFo* **2014**, *186*, 1094−1101.

DOI: 10.1021/am508118x
ACS Appl. Mater. Interfaces 2015, 7, 2847−2855